Int. J. Nano Dimens., 14 (1): 103-114, Winter 2023

ORIGINAL ARTICLE

Synthesis and characterization of Iron Oxide, rare earth Erbium Oxide, and Erbium Oxide blended Iron Oxide nanocomposites for biomedical activity application

Umadevi Palani[1], Baskaran Iruson[1], Sathyaseelan Balaraman[2], Senthilnathan Krishnamoorthy[3], Manikandan Elayaperumal[4]*

[1]*Department of Physics, Arignar Anna Govt. Arts College, (Affiliated: Thiruvalluvar University, Vellore), Tamil Nadu (TN), India*
[2]*Department of Physics, University College of Engineering Arni, Anna University Chennai, TN, India*
[3]*Department of Physics, VIT University, TN, India*
[4]*Department of Physics, Thiruvalluvar University, TVUCAS Campus, Thennangur, Tamil Nadu, India*

Received 06 August 2022; revised 22 October 2022; accepted 30 October 2022; available online 03 November 2022

Abstract
In this report, we intend to synthesize iron oxide (Fe_2O_3), erbium oxide (Er_2O_3), and a composite of erbium oxide/iron oxide (Er_2O_3/Fe_2O_3) nanoparticles (NPs) by a microwave irradiation technique. After the synthesis, we explore the various physicochemical properties of the sample with the help of various systematic characterization techniques. First, the prepared sample has been subjected to XRD for determining the crystal structure. Then, we confirm the functional groups of the sample with the help of FTIR. Further, we analyze the absorbance and the band gap with a UV-Vis spectrometer. Besides, we also investigate the microbial studies, namely, the anti-bacterial and the anti-fungal. Finally, we also analyze the response of human breast cancer cells when they are exposed to iron oxide (Fe_2O_3), erbium oxide (Er_2O_3), and a composite of erbium oxide/iron oxide (Er_2O_3/Fe_2O_3) nanoparticles (NPs) with MDA MB 231 by MTT assay.

Keywords: *Biomedical Activity; Microwave Synthesis; Nanostructures; Optical; Structural; Transition/Rare Earth Oxides.*

How to cite this article
Palani U., Iruson B., Balaraman S., Krishnamoorthy S., Elayaperumal M. Synthesis and characterization of Iron Oxide, rare earth Erbium Oxide, and Erbium Oxide blended Iron Oxide nanocomposites for biomedical activity application. Int. J. Nano Dimens., 2023; 14(1): 103-114.

INTRODUCTION

It is well known that it was Richard Feynman who pondered the idea of nano-technology in 1959. Technology has penetrated almost all the fields of science, engineering, medicine, etc. So far, various types of nanoparticles have been synthesized and they found immense applications, especially, in nano-biotechnology, for instance, several outstanding nanomedicines (chemotherapeutic agents, biological agents, immunotherapeutic agents, etc.) in the treatment of various diseases [1.2] and vaccine administration [3]. In recent decades, the interest has turned towards synthesizing the various metal oxide nanoparticles as metal oxides, in general, play an indispensable role in many areas of physics, chemistry, and materials science. Further, these oxides are widely utilized for fabricating piezoelectric devices, fuel cells, microelectronic circuits, sensors, coating surfaces against corrosion, and catalysts. The metal oxides exhibit metallic, semiconductor, or insulator behaviors as they facilitate structural geometries with an electronic structure. To date, several chemical synthesis methods have been proposed, namely, chemical vapor deposition, co-precipitation, sol-gel, and microwave irradiation methods for fabricating the various types of nanoparticles [4, 5]. Microwave-assisted amalgamation has attracted much attention because it has the advantages of being quicker, meeker, and more energy efficient [6, 7]. In the microwave-assisted sol-gel method, the precursor

* Corresponding Author Email: bsseelan03@gmail.com

solution is exposed to a microwave source. The efficient energy transfer can result in a rapid heating route. Furthermore, microwave heating can result in the homogeneous heating of the metal oxide in a rather short time to achieve a uniform distribution of particle size [8, 9]. From the recent literature survey, it has been reported that different types of Fe_2O_3, Er_2O_3, and Er_2O_3/Fe_2O_3 nanoparticles have been synthesized and they exhibited outstanding antibacterial properties against various types of bacteria of Bacillus SP, *S. marcescens, C. albicans, S. aureus, E. coli, P. aeruginosa, B. subtilis, M. varians, A. flavus*, etc. These nanoparticles can induce membrane stress through direct contact with the walls of bacterial cells. Hence, they damage and disrupt the cell membranes. Eventually, this leads to cell death. It should be emphasized that Aspergillus and Mucor commonly affect plant product materials rather than humans [10-13]. These postharvest pathogenic fungi have been recovered by using these Fe_2O_3, Er_2O_3, and Er_2O_3/Fe_2O_3 nanoparticles [14]. Thus, the composite Er_2O_3/Fe_2O_3 nanoparticles inhibit more of those fungi when compared to the Fe_2O_3 and Er_2O_3 nanoparticles. Therefore, in this work, we intend to synthesize the iron oxide nanoparticles, the erbium oxide nanoparticles, and finally the composite of erbium-doped iron oxide nanoparticles by microwave irradiation technique, which was introduced in the 1980s. It is well established that this technique significantly increases yields, reduces reaction time, and reduces side reaction's energy efficiency and greener process. Besides, microwave heating provides several benefits when compared to conventional heating methods [15, 16]. Further, we find that the Fe_2O_3, Er_2O_3, and Er_2O_3/Fe_2O_3 NPs as composites synthesized by microwave irradiation exhibit cytotoxic effects in breast cancer cells without harming the healthy cells.

MATERIALS AND METHODS

To synthesize the iron oxide (Fe_2O_3), erbium oxide (Er_2O_3), and a composite of erbium oxide doped with iron oxide (Er_2O_3/Fe_2O_3) nanoparticles (NPs), all the required chemicals $Fe(NO_3)_2.9H_2O$ (99.6 %), $Er(NO_3)_3.5H_2O$(99.6%) and Urea (NH_2CONH_2) were purchased from Sigma-Aldrich. Iron oxide (Fe_2O_3), erbium oxide (Er_2O_3), and a composite of erbium oxide doped with iron oxide (Er_2O_3/Fe_2O_3) nanopowder were prepared by the microwave sintered method. The sample $Fe(NO_3)_2.9H_2O$, and NH_2CONH_2, $Er(NO_3)_3.5H_2O$(99.6%), and Urea (NH_2CONH_2) and $Fe(NO_3)_2.9H_2O$ with $Er(NO_3)_3.5H_2O$ as a composite both were taken in equal ratio 1:1 with their stoichiometry prepared from the raw materials. The purchased materials were weighed and mixed according to the stoichiometric ratio. The powders were pressed into the disk-shaped cakes using the hydraulic press. These were pre-sintered at a temperature of 800˚C for 30 min. in a microwave furnace (V.B. Ceramics India, 2.45 GHz frequency with a power output of 2.2 kW). The pre-sintered cakes were removed from the microwave furnace and crushed into powder. These samples were ground for 1hr in an agate mortar to make them into fine powder possessing uniform particle size. The obtained material was subjected to different characterizations to confirm the appropriateness of the device application.

Characterization Techniques

Powder X-ray diffraction (XRD) measurements were carried out for iron oxide, erbium oxide, and erbium-doped iron oxide samples using a Bruker D8 Advance diffractometer with monochromatized Cu Kα radiation (λ=1.5418 Å). The X-ray source was operated at 40 kV with a current of 40 mA. The measurements were performed by θ - 2θ scans in the 2θ range 20-80° with a step size of 0.02 degrees and a scan speed of 0.1 seconds per step. The FT-IR analysis has been done with a Perkin Elmer set of BXII models in a range of 4000 - 400 cm^{-1}. The optical spectra of the samples were recorded by UV-Vis spectrometer of Jasco model no- V – 670. The PL measurements were carried out at room temperature using 275 nm wavelength as excitation wavelength with a Hitachi f-4500 FL spectrophotometer where a xenon lamp was used as an excitation source.

Test Microorganisms

Aspergillus Mucor fungi were used for carrying out antimicrobial activity studies. These microorganisms were grown for 3 days at 37 °C in *Actinomyces* Isolation Media (AIM) broth (Himedia, Mumbai, India). The sensitivity of these microorganisms to the reference antibiotics was checked using myostatin as a positive control.

Antifungal Activity of the Sample

The samples of iron oxide, erbium oxide, and iron oxide/erbium oxide nanoparticles were loaded on Potato Dextrose agar plates at three different

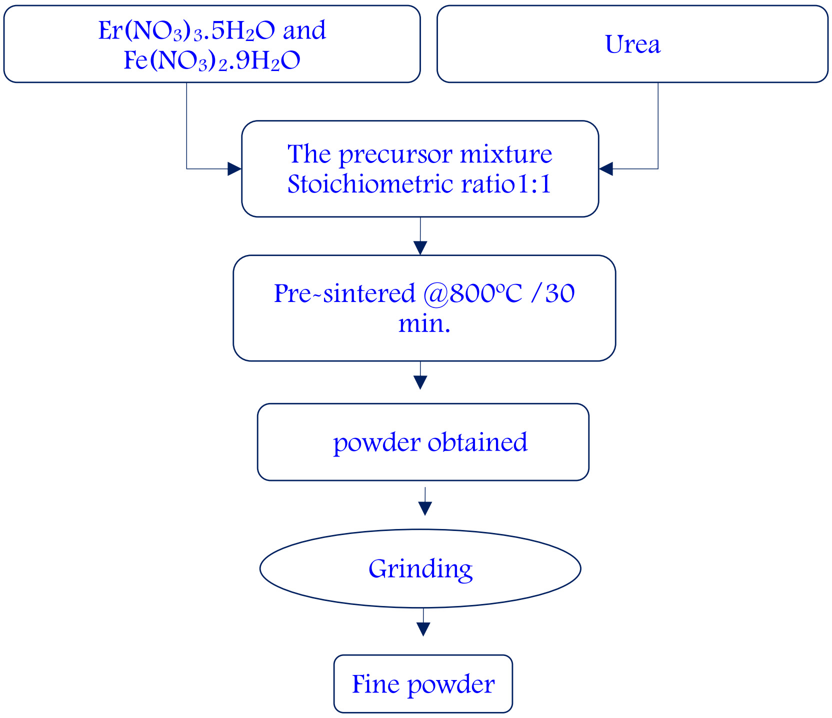

Fig. 1. Flow chart of synthesis of Fe_2O_3, $Er_2O_3$and Er_2O_3/Fe_2O_3 NPs.

volumes (10, 20, and 30 µl) and swabbed with fungi such as *Aspergillus* and *Mucor*. Antifungal activities of the samples were determined by the good diffusion method on Potato Dextrose Agar (PDA) medium [13]. The PDA medium was composed of (gl^{-1}) potato infusion-200, dextrose -20, and agar-15. The PDA medium was poured into the Petri plate; and after solidification, the inoculum was spread on the PDA plates with a sterile swab moistened with the fungal suspension. All the plates were incubated at 37 °C for 3 days and finally, the inhibition zone was analyzed. These fungi were grown in Actinomyces Isolation Media (AIM) broth (HIMEDIA Mumbai). Myostatin was used as the positive control to check the sensitivity against antibiotics by the well diffusion method on the PDA medium.

Antibacterial Activity of the Sample

The antibacterial activity of iron oxide, erbium oxide, and iron oxide/erbium oxide nanoparticles was tested against Escherichia coli, and Bacillus sp using the disc diffusion method. The iron oxide, erbium oxide, and iron oxide/erbium oxide nanoparticles were prepared at an appropriate concentration of 1 mg/ml with dimethylsulfoxide solution for this process. Then, the dispersed nanoparticles were impregnated on each sterile disc by using a micropipette. After that, the discs were kept on culture swapped Mueller Hinton Agar medium using sterile force, and allowed to incubate for 24 hrs. The average zone of inhibition diameter was measured in millimeters (mm).

Cell Culture and Cell Line Maintenance

The human breast cancer cell lines MDA MB-231 were obtained. Then, these cell lines were grown as a monolayer in Dulbecco's modified Eagle's medium (DMEM: Hi Media Laboratories, Mumbai, India), which was supplemented with 10% fetal bovine serum, 100 U/mL penicillin, and 100 µg/mL streptomycin (Hi-Media Laboratories Mumbai, India) cells grown at 37˚C in an incubator under 5% CO_2 with high humidity [17].

MTT Assay Method for Evaluation of Cell Viability and Cytotoxicity

The anticancer activity of samples on human breast cancer cell lines MDA MB-231 was determined by the MTT (3-(4, 5-dimethyl thiazol-2yl)-2, 5-diphenyl tetrazolium bromide) assay[34,35]. These cells (1 × 10^5/well) were plated in 0.2 ml of the cells with a concentration of 1 × 105 cells/ml. The plates were incubated for 24 hrs in a 5%

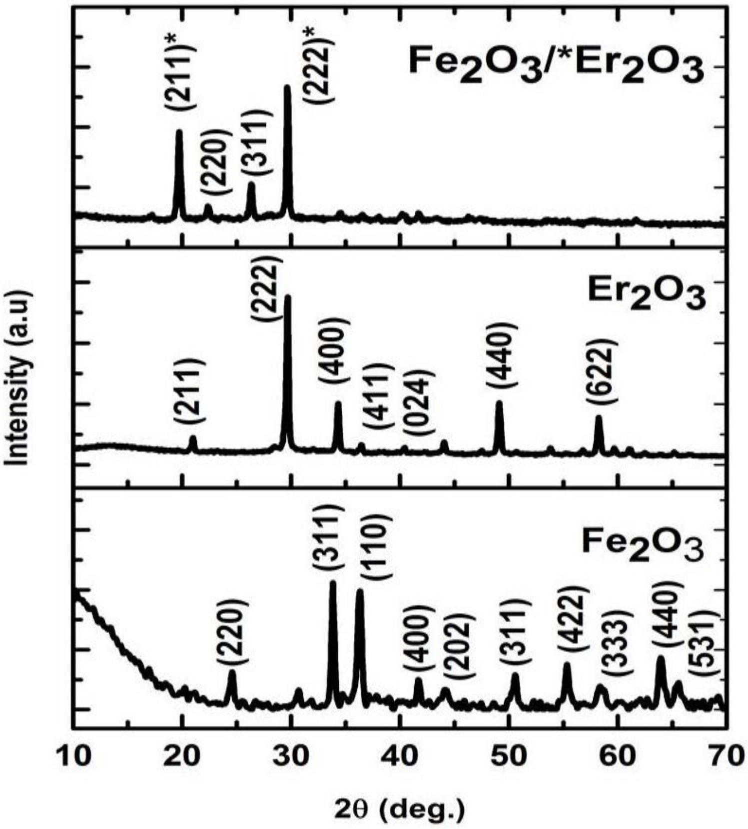

Fig. 2. XRD pattern of Fe_2O_3, $Er_2O_3$and Er_2O_3/Fe_2O_3 NPs.

CO_2 incubator for cytotoxicity. After incubation, normal breast (MDA MB-231) cells were cultured in a 1:1 mixture of dimethyl sulfoxide (DMSO). Then, they were added to each well and mixed well by micropipette[36]. The percentage of viable cells was visualized by the development of purple color due to the formation of formazan crystals. The suspension was transferred to the cuvette of a spectrophotometer and observed significant variance/instability in the optical density (OD) was. Measurements were performed and the concentration required for a 50 % inhibition of viability (IC_{50}) was determined and used for the bioassays.

RESULTS AND DISCUSSION

Structural Analysis

Fig. 1 shows the XRD pattern of the sample prepared by Microwave-assisted synthesis methods. XRD patterns analyzed by the particle size and the crystal structure are shown in Fig. 2 Here, the XRD pattern can be indexed well to the rhombohedral structure of Fe_2O_3 (JCPDS 89-2810) where the diffraction peaks are found at 24.22º, 33.23º, 35.53º, 40.77º, 49.25º, 54.04º and 62.71º with corresponding to (220), (311), (110), (400), (202), (311) and (214) plane, respectively. The particle size is calculated by using Scherrer's formula [18] given below,

$$D_{XRD} = \frac{0.9\lambda}{\beta\cos\theta_{\beta}} \tag{1}$$

where λ is the x-ray wavelength (Cu Kα = 1.5418Å), k is a constant (0.916), β is the full width at half maximum (FWHM) of the peak, and θ is the Bragg angle peak position. The lattice constants for Fe_2O_3 nanoparticles are a = b = 5.040 Å and c = 13.74650 Å and the average crystal size has been calculated as 12 nm**.** From JCPDF chart 77-0777, the XRD confirmed that Er_2O_3 possesses the cubic structure. By applying Scherrer's formula [19], the FWHM for the strongest reflection peak of (222) with cell parameters a = 10.53 Å, the particle size was calculated to be 15 nm**.** Further, the XRD pattern was also analyzed for the erbium-doped iron composite material. It has been found that the peaks of iron oxide and erbium oxide are shifted to a new position when they are used as a composite;

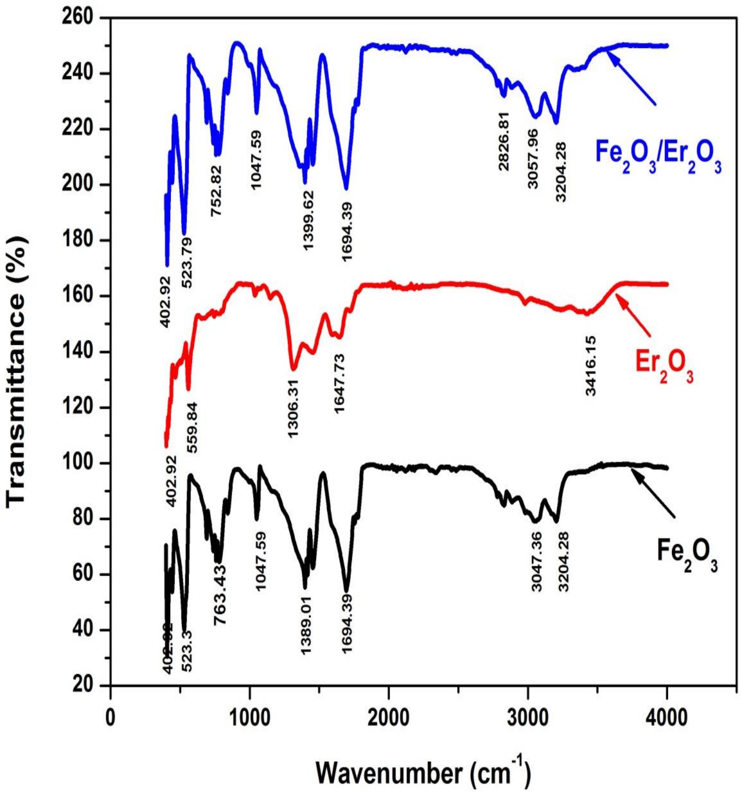

Fig.3. FTIR spectrum for the presence of functional groups of Fe_2O_3, $Er_2O_3$and Er_2O_3/Fe_2O_3 NPs.

the particle size was calculated to be 17 nm.

Fourier transforms infrared spectroscopy (FTIR) Studies

The FTIR spectra of Fe_2O_3, $Er_2O_{3,}$ and Er_2O_3/Fe_2O_3 NPs were shown in Fig. 3 where the three spectra were combined and the functional groups were also analyzed. The functional groups present in the three were compared and found the peaks ranging from 406 cm^{-1} to 555.49 cm^{-1} have the halogen compounds, the peaks of 769.97 cm^{-1} and 759.95 cm^{-1} of iron oxide and iron oxide composited with Erbium oxide have the halogen compound. Peaks of 530.42 – 528.48 cm^{-1} and 555.49 cm^{-1} show the flattened peak of Fe-O and Er-O bonds for metal oxides (M-O) [19]. The absorption band of 109.27 cm^{-1} is due to the vibration of crystalline Fe-O modes [20]. The broadband at 3203.76 - 3069.10 cm^{-1} may be assigned to OH stretching vibration of the hydroxyl group. The band at 1643.36 and 1693.60 cm^{-1}correspond to C-O stretching vibration and C = O symmetry, respectively. FTIR functional information gives the justification for good chemical properties and is consistent with the XRD pattern [21].

Optical Absorption Spectral Studies

An optical absorption spectrum of the Fe_2O_3, $Er_2O_3$and Er_2O_3/Fe_2O_3 NPs was carried out between 300 to 900 nm using a UV visible spectrometer and the results are shown in Fig. 4(a). The optical studies reveal that the absorption peaks were found to be 377 nm for Fe_2O_3 NPs. For Er_2O_3 NPs, the absorption peaks were found to be 204, 379, 519, 655, 802, 976, and 1520 nm. Similarly, for Er_2O_3/Fe_2O_3 NPs, the band peaks were present at 348 nm [22].

Owing to the direct band gap, Fe_2O_3, $Er_2O_3$and Er_2O_3/Fe_2O_3 NPs under study have an absorption coefficient (α) obeying the following relation for high photon energies (hν);

$$\alpha = \frac{(h\upsilon - E_g)^{1/2}}{h\upsilon} \tag{2}$$

Here, E_g is the optical band gap, *h* is Planck's constant, and ν is the frequency of the incident light. The variation of $(\alpha h\nu)^2$ against hν is shown in fig. 4(b). The E_g is evaluated by the extrapolation of the linear part and the band gap for Fe_2O_3, $Er_2O_3$and for Er_2O_3/Fe_2O_3 NPs was found to be 2.07, 4.85, and 2.33 eV, respectively [23, 24].

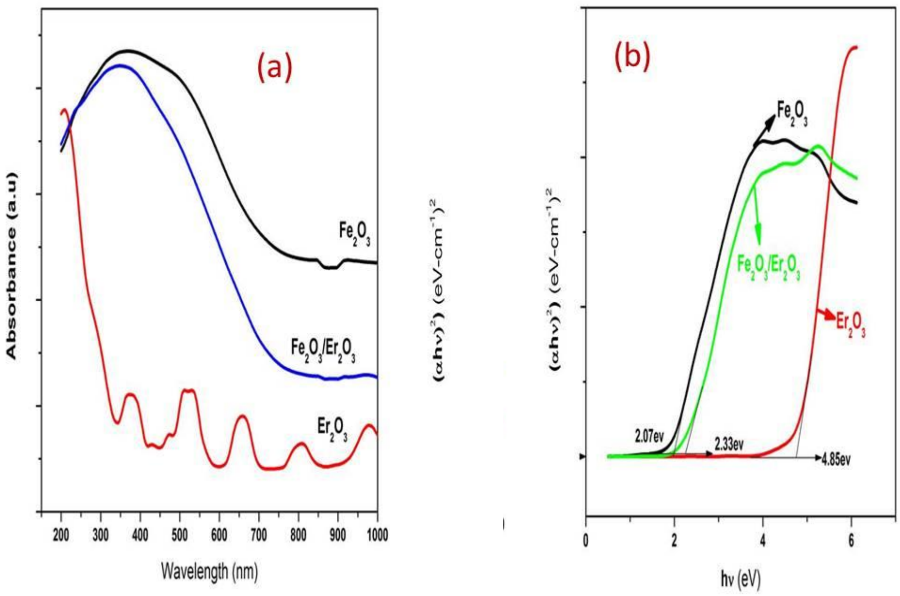

Fig . 4. UV Absorption bands of (a) Fe_2O_3, $Er_2O_3$and Er_2O_3/Fe_2O_3 NPs and UV band gap for (b) Fe_2O_3, $Er_2O_3$and Er_2O_3/Fe_2O_3 NPs.

Photoluminescence Spectra

Photoluminescence (PL) spectroscopy is a suitable technique to determine the crystalline quality and the exciton fine structure. Fig. 5 represents the PL spectrum of Fe_2O_3, Er_2O_3, and Fe_2O_3/Er_2O_3 as a composite nanoparticle at room temperature. The sample exhibits two strong emission bands, namely, blue and blue-green emissions at 368 and 438 nm, respectively. These peaks are due to structural defects' existence including oxygen vacancies and the results are consistent with the earlier reports [25]. The recorded spectra show sharp PL peaks for green and red centered at about 654, 656, 668, and 733 nm due to the phonon-assisted population mechanism of transition of Fe^{3+} and Er^{3+}[26, 27]

Anti-bacterial Studies

As prepared samples of Fe_2O_3, Er_2O_3, and Er_2O_3/Fe_2O_3 NPs against *E. coli* (Gram –ve) and Bacillus sp (Gram +ve) show good antibacterial activity [28]. The mechanism of transition of Fe^{3+} and Er^{3+} results in the generation of more reactive and potent oxygen species [29, 30].

A sample with Fe_2O_3nanoparticles of 100 µl demonstrated higher activity against Bacillus sp and the inhibition zone was 12 mm, followed by *E. coli* whose inhibition zone was found to be 19 mm,

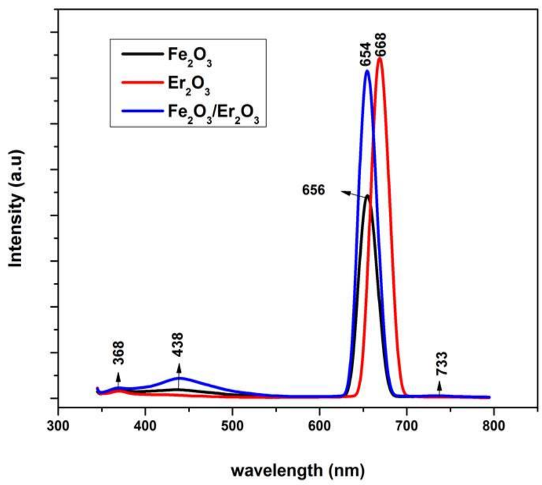

Fig. 5. Photo Luminescence of Fe_2O_3, $Er_2O_3$and Er_2O_3/Fe_2O_3 NPs.

Table 1. Antibacterial activity of samples against bacteria.

S.No	Samples	Bacteria organism	Zone of inhibition (mm)			
			100mg	200mg	300mg	Control (streptomycin antibiotic)
1	Fe_2O_3/ Er_2O_3	Bacillus sp (g +ve)	21mm	23mm	27mm	24mm
		E coli (g - ve)	21mm	22mm	23mm	19mm
2	Fe_2O_3	Bacillus sp (g +ve)	12mm	15mm	18mm	20mm
		E coli (g - ve)	19mm	20mm	22mm	23mm
3	Er_2O_3	Bacillus sp (g +ve)	19mm	22mm	23mm	14mm
		E coli (g - ve)	13mm	15mm	18mm	22mm

respectively. The iron oxide nanoparticles of 200 µl and 300 µl demonstrated an increasing tendency of the inhibition zone and the details are presented in Table1. Similarly, the antibacterial activity of Fe_2O_3 nanoparticles against the bacteria such as Bacillus sp, and *E. coli* is shown in figs. 6(a) and 6(d).

From figs. 6(b) and 6(e) and table1, it can be observed that the sample with Er_2O_3 nanoparticles of 100 µl was active against Bacillus sp, and the inhibition zone was 19 mm, followed by *E. coli* whose inhibition zone is 13 mm. When the concentration of the sample increases to 200 µl, the sample was active against bacteria but the inhibition zone increases to 22 mm against Bacillus sp and 15 mm against *E. coli*. Finally, the inhibition zone is 23 mm in 300 µl extract for Bacillus sp which is higher than the standard value. In the case of *E. coli*, the inhibition rises to 15 mm was observed.

From figs. 6(c) and 6(f) and table1, it has been found that the sample (Fe_2O_3/Er_2O_3 nanoparticles) of 100 µl was active against Bacillus sp, and the inhibition zone was 21 mm, followed by *E. coli* whose inhibition zone was 21 mm. When the concentration of the sample is increased to 200 µl, the sample was active against bacteria but the inhibition zone increases to 23 mm against Bacillus sp and 22 mm against *E. coli*. However, for the sample with 300 µl, the sample was active and the inhibition zone is 27 mm for Bacillus sp which is higher than the standard value. In the case of *E. coli*, the enhanced inhibition of 23 mm was observed.

It is envisaged that there exists an electrostatic interaction between positively charged nanoparticles and negatively charged bacteria. Owing to this, the small-sized nanoparticles penetrate inside the cell wall and eventually cause cell damage. During the generation of reactive oxygen species (ROS), small-sized particles of constituent ions are released through a reflux mechanism [31]. Therefore, the antibacterial activity of the Fe_2O_3, Er_2O_3, and Fe_2O_3/Er_2O_3 was found to be enhanced rate.

Anti-Fungal Studies

The antifungal activity of Fe_2O_3, $Er_2O_3$and Er_2O_3/ Fe_2O_3 NPs is carried out. The nanoparticles were also subjected to the evaluation of their antifungal activities against different strains such as *Aspergillus* and *Mucor* with different concentrations.

A sample with Fe_2O_3 nanoparticles of 100 µl demonstrated higher activity against *Aspergillus* and the inhibition zone was 11 mm, followed by *Mucor* whose inhibition zone was found to be 18 mm. The iron oxide nanoparticles of 200 µl and 300 µl demonstrated an increasing tendency of the inhibition zone and the detailed results are presented in Table.2. Similarly, the antifungal activity of iron oxide nanoparticles against the fungi such as *Aspergillus*, and *Mucor* is shown in figs. 7(a) and 7(d).

From figs. 7(b) and 7(e) and table 1, it has been observed that the Er_2O_3 nanoparticles with 100 µl were active against *Aspergillus* and the inhibition zone was 18 mm and the *Mucor*'s inhibition zone was 13 mm. When the concentration of the sample is increased to 200 µl, the sample was also active against fungi but the inhibition zone is increased to 21 mm against *Aspergillus* but 14 mm against *Mucor*. However, for 300 µl extract, the inhibition zone was found to be 22 mm for *Aspergillus* and this is higher than the standard value. In the case of *Mucor*, the inhibition has been raised to 17 mm.

From figs. 7(c) and 7(f), and table 2, it is seen that the Er_20_3/ Fe_2O_3nanoparticles of 100 µl were

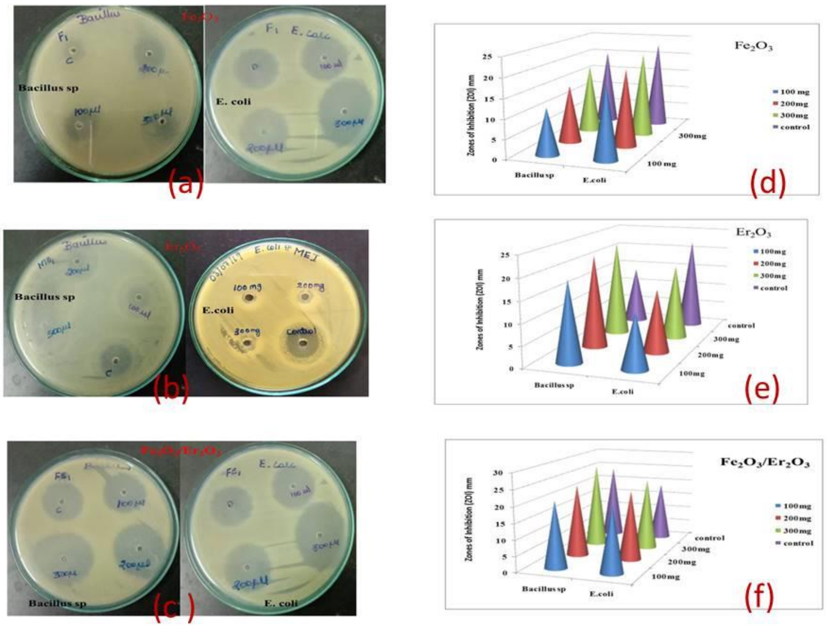

Fig. 6. Anti-bacterial activity comparison of Zones of Inhibition (ZOI) Bacillus sp (G+ve) and *E. coli* (G-ve) (a) Fe_2O_3,(b) $Er_2O_3$and (c) Er_2O_3/Fe_2O_3 NPs and Anti-bacterial activity (d) Fe_2O_3, (e) $Er_2O_3$and (f) Er_2O_3/Fe_2O_3 NPs.

active against *Aspergillus* and the inhibition zone was 13 mm, followed by *Mucor* whose inhibition zone was 15 mm. When the concentration of the sample is increased to 200 µl, still the sample was active against fungi and the inhibition zone was extended to 19 mm against *Aspergillus* but 16 mm against *Mucor*. Lastly, for 300 µl, the sample was still active for *Aspergillus* and the inhibition zone was 21 mm which is higher than the standard value. In the case of *Mucor*, the inhibition has been extended to 16 mm.

The size of the bacteria/microbes is typically in the order of micrometers [32, 33]. Nearly, thousands of nanoporous were found in their outer cellular membranes. At this juncture, it should be emphasized that the size of the particle of the iron oxide and erbium oxide, and Fe_2O_3/Er_2O_3 is less than 100 nm, and they are unlikely to enter the cell wall and damage the fungi from the interior. In addition, the liberated metal ions from the doped nanoparticle may also impact the antifungal activity by disrupting the cell membrane and gaining entry [34].

Cytotoxicity and cell viability analysis of MDA MB-231 cell line

In the last two decades, there has been immense interest in the pharmacological effects of bioactive compounds on cancer treatments and prevention. The research investigations reveal that there are numerous anti-cancer activities in various cancer cells through different forms of cytotoxic effects without exhibiting considerable damage to normal cells [31-33]. In vitro cytotoxic

Table 2. Anti fungal activity of samples against fungus.

S.No.	SAMPLES	FUNGUS ORGANISM	ZONE OF INHIBITION (mm)			
			100mg	200mg	300mg	CONTROL
1	Fe_2O_3/ Er_2O_3	ASPERGILLUS	13mm	19mm	21mm	16mm
		MUCOR	15mm	16mm	16mm	12mm
2	Fe_2O_3	ASPERGILLUS	11mm	14mm	17mm	19mm
		MUCOR	18mm	19mm	21mm	22mm
3	Er_2O_3	ASPERGILLUS	18mm	21mm	22mm	13mm
		MUCOR	13mm	14mm	17mm	21mm

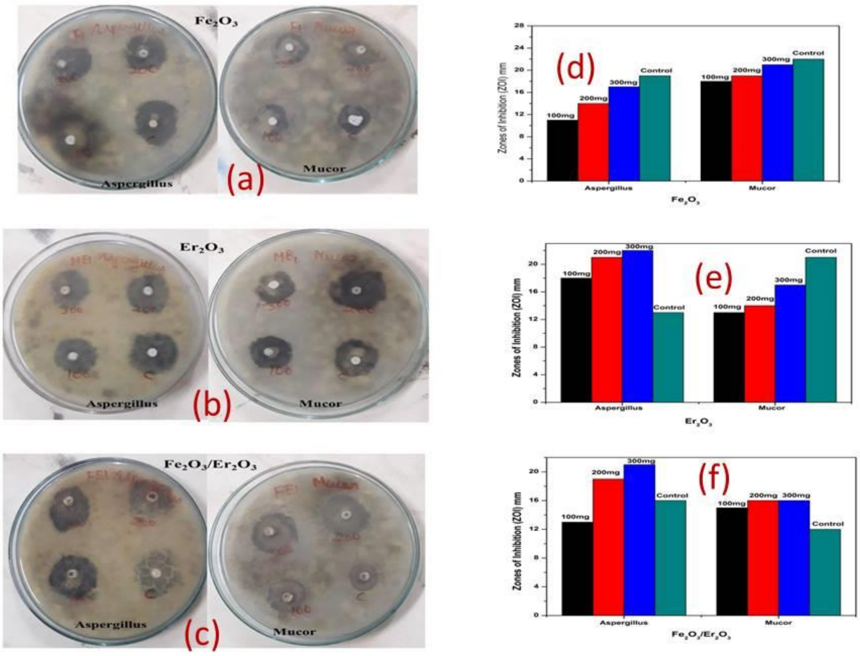

Fig. 7. Anti- fungal activity comparison of Zones of Inhibition *Aspergillus* and *Mucor* organism (a) Fe_2O_3, (b) Er_2O_3, and (c) Er_2O_3/Fe_2O_3 NPs and Anti- fungal activity (d) Fe_2O_3, (e) Er_2O_3 and (f) Er_2O_3/Fe_2O_3 NPs.

potential of Fe_2O_3, Er_2O_3 and Er_2O_3/Fe_2O_3 NPs and human breast cancer MDA MB-231 cell line and viability of tumor cells were confirmed using MTT assay. When the cells were treated with various concentrations (0, 5, 10, 25, 50, 75, and 100 µg/mL) of iron oxide, erbium oxide, and Fe_2O_3/Er_2O_3 NPs for 24 hrs, a significant decrease in cell viability was observed when compared to untreated cells whose viability is assumed to be 1 (i.e.,100 %). In this study, various percentages of cell viability were examined in cultured cells. The results showed that Fe_2O_3, Er_2O_3 and Er_2O_3/Fe_2O_3 NPs induced significant potential cytotoxic response which is depicted in Figs. 8(a-d). Further, all these details are also clearly presented in Table 3. Upon treatment of the MDA MB-231 cells with Fe_2O_3NPs for 24 hrs at 37 °C with a concentration of 5 µg/mL, maximum cell viability of 20% has been noticed. In the case of MDA MB-231 cells with Er_2O_3NPs for 24 hrs at 37 °C, maximum cell viability of 17% has been observed for a concentration of 50 µg/mL. Finally, when MDA MB-231 cells are treated with a composite of Fe_2O_3 and Er_2O_3NPs, maximum cell viability of 21% has been noted for a concentration of 75 µg/mL. Thus, based on the above discussions, a noticeable dose-dependent reduction in cell viability has been observed. Consequently, the results of the MTT assay demonstrated that iron oxide, erbium oxide, and Fe_2O_3/Er_2O_3 NPs have appreciable effects on human breast cancer MDA MB-231 cells [35-40]. Thus, these results revealed the non-toxic nature and best biocompatibility of our synthesized Fe_2O_3, Er_2O_3 and Er_2O_3/Fe_2O_3 NPs in vitro experiments against normal cell MDA MB-231 and their toxic nature against cancerous cells. The outcomes of our study conform to the modern fact that the mainly employed biocompatible material for the preparation of nanoparticles. Interestingly, Fe_2O_3, Er_2O_3, and Er_2O_3/Fe_2O_3 NPs have not exerted a significant toxic effect as >80 % viability of normal cells MCF-10A at the highest concentration, whereas human breast cancer MDA MB-231 cancerous cells show the profound cytotoxic effect. Therefore, it is suggested that the severe cytotoxicity mostly is initiated by the cellular internalization of Fe_2O_3, Er_2O_3, and Er_2O_3/Fe_2O_3 NPs instead of physical injury to the cell membrane.

From the result anti-cancer, the cytotoxic effect for the samples demonstrated that metal oxide nanoparticles show cytotoxicity by inducing apoptosis in MDA-MB231 breast cancer cells. However, further studies are needed to increase the therapeutic potential of metal oxide nanoparticles to a much higher extent by functionalizing them with targeting by encapsulation with other drugs. It would be interesting to study the mechanism

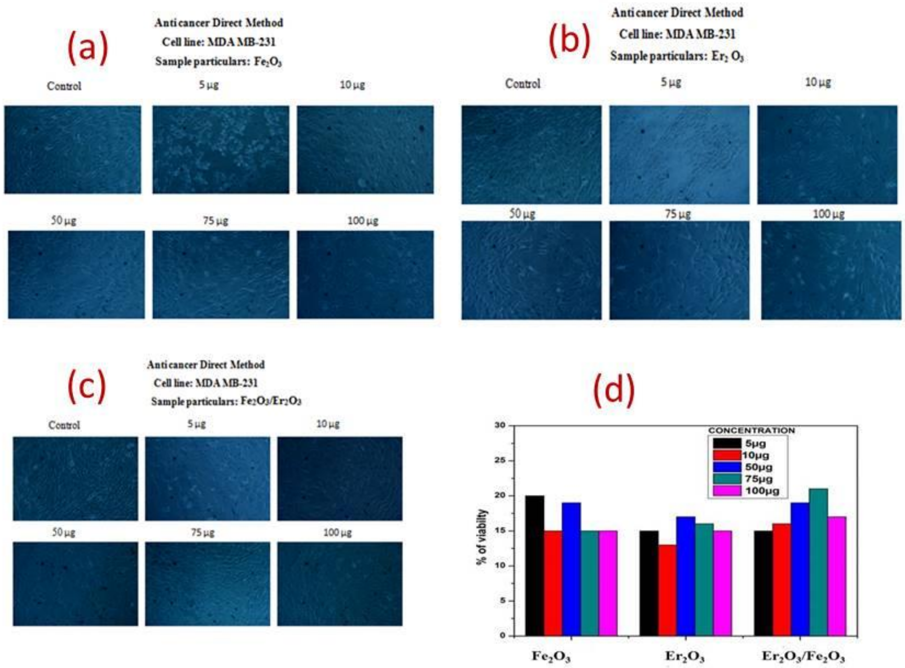

Fig. 8. Anti-cancer activity (a) Fe_2O_3, (b) Er_2O_3 and (c) Er_2O_3/Fe_2O_3 NPs and anti-cancer plot for (d) Fe_2O_3, Er_2O_3 and Er_2O_3/Fe_2O_3 NPs.

of metal oxide nanoparticles to formulate a more potent and effective anticancer drug.

CONCLUSION

In this report, the nanoparticles of Fe_2O_3, Er_2O_3, and Er_2O_3/Fe_2O_3 were successfully synthesized by the microwave synthesis method. By analyzing the XRD pattern with the help of Scherrer's formula, the size of the nanoparticles has been determined to be 12 nm, 15 nm and 17 nm for Fe_2O_3 and Er_2O_3 and Er_2O_3/Fe_2O_3, respectively. The band gaps have been calculated from the Tauc Plots which have been plotted from the data of UV-Vis spectroscopy. Further, the photoluminescence emission spectra of Fe_2O_3, Er_2O_3, and Er_2O_3/Fe_2O_3 NPs exhibited an active blue-green emission and underwent a red shift owing to oxygen vacancies ions. In addition to the above studies, antifungal activity

Table 3. Anti-cancer activity of samples against cancer.

Sample particulars		Cytotoxity (%)	Cell Viability (%)	Cytotoxic Reactivity
Description	Conc.(µg)			
Fe_2O_3	5	80	20	severe
	10	85	15	severe
	50	81	19	severe
	75	85	15	severe
	100	85	15	severe
Er_2O_3	5	85	15	severe
	10	87	13	severe
	50	83	17	severe
	75	84	16	severe
	100	85	15	severe
Fe_2O_3/Er_2O_3	5	84	15	severe
	10	84	16	severe
	50	81	19	severe
	75	79	21	severe
	100	83	17	severe

of Fe_2O_3, Er_2O_3 and Er_2O_3/Fe_2O_3 nanoparticles has been carried out against postharvest pathogenic fungi such as *Aspergillus* and *Mucor*. It has been found that the composite of Er_2O_3 doped Fe_2O_3 nanoparticles enhances the inhibition zone for all fungal pathogens when compared to the individual iron oxide and erbium oxide nanoparticles. Finally, in vitro cell viability tests using an MTT assay revealed that the synthesized nanoparticles possess a great anti-cancer potential against cancerous cell lines but they have no significant toxic effect on normal cells.

ACKNOWLEDGMENTS

Financial support from the Tamilnadu State Council for Science and Technology under grant number, C. No. TNSCST/STP-PRG/AR/2018-2019/9333 this part of a research program to whom we are gratefully acknowledged.

CONFLICT OF INTEREST

The authors declare no conflict of interest.

ETHICAL APPROVAL

This article does not contain any studies with human participants or animals performed by any of the authors.

REFERENCES

1. Siegel R. L., Miller K. D., Fuchs H. E., Jemal A. (2021), Cancer Statistics. *CA Cancer J. Clin.* 71: 7–33.
2. Jain S., Hirst D. G., O'Sullivan J. M., (2012), Gold nanoparticles as novel agents for cancer therapy. Br. J. Radiol. 85: 101–113.
3. Heidi H., Prechl J., Jiang H., Zozulya A., Fabry Z., Denes F., Sandor M., (2010), Using carbon magnetic nanoparticles to target, track, and manipulate dendritic cells. *J. Immunol. Methods*. 356: 47-59.
4. Mohammadi S. Z., Motlagh K., Jahani S., Yousefi M., (2012), Synthesis and characterization of α-Fe_2O_3 nanoparticles by microwave method. *Int. J. NanoSci. Nanotechnol.* 8: 87-92.
5. Sathyaseelan B., Senthilnathan K., Alagesan T., Jayavel R., Sivakumar K., (2010), A study on structural and optical properties of Mn-and Co-doped SnO_2 nanocrystallites. *Mater. Chem. Phys.* 124: 1046-1050.
6. Krishnakumar T., Jayaprakash R., Parthibavarman M., Phani A. R., Singh V. N., Mehta B. R., (2009), Microwave-assisted synthesis and investigation of SnO_2 nanoparticles. Mater. Lett. 63: 896-898.
7. Davoodnia A., Rahimizadeh M., Atapour-Mashhad H., Tavakoli-Hoseini N., (2009), Investigation into the reaction of 2-amino-4, 5-dimethylthiophene-3-carboxamide with iso (and isothio) cyanates under microwave irradiation. Heteroatom Chem.: An Int. J. Main Group Elem. 20: 346-349.
8. Parida K. M., Parija S., (2006), Photocatalytic degradation of phenol under solar radiation using microwave irradiated zinc oxide. *Solar Energy*. 80: 1048-1054.
9. Mirzaei H., Davoodnia A., (2012), Microwave-assisted sol-gel synthesis of MgO nanoparticles and their catalytic activity in the synthesis of hantzsch 1, 4-dihydropyridines. Chin. J. Catal. 33: 1502-1507.
10. Devendra K., Himani Sh., Neelam Sh., (2022), Antibacterial and morphological studies of plant-mediated synthesized CuO nanoparticles using *Azadirachta indica (neem)* leaf extract. *Int. J. Nano Dimens.* 13: 197-204.
11. Preethi S., Zhang X., Hao G., Joly A. G., Singh S., Hossu M., Sun X., Chen W., (2019), Folic acid-CdTe quantum dot conjugates and their applications for cancer cell targeting. *Cancer Nanotechnol.* 1: 19-24.
12. Maryam M., Anthony D. M., Hoskins C., (2014), The use of iron oxide nanoparticles for pancreatic cancer therapy. *J. Nanomed. Res.* 1: 00004.
13. Kanagesan S. M., Hashim S., Tamilselvan N. B., Alitheen I., Hajalilou A., Ahsanul K., (2013), Synthesis, characterization, and cytotoxicity of iron oxide nanoparticles. *Adv. Mater. Sci. Eng.* 2013: Article ID 710432.
14. Shameera Begum B. A., Farida B. I., Hemalatha S., (2021), Cancer nanomedicine: A review on approaches and applications towards targeted drug delivery. *Int. J. Nano Dimens.* 12: 310-327.
15. Sasikala C., Suresh G., Durairaj N., Baskaran I., Sathyaseelan B., Kumar M., Senthilnathan K., Manikandand E., (2020), Influences of Ti^{4+} ion on dielectric property in perovskite structure of La Ferrite (LaFe1-X $TiXO_3$). *J. Alloys and Comp.* 845: 155040-155045.
16. Sasikala C., Suresh G., Durairaj N., Baskaran I., Sathyaseelan B., Manikandan E., Srinivasan R., Moodley M. K., (2019), Chemical, morphological, structural, optical, and magnetic properties of transition metal titanium (Ti)-doped $LaFeO_3$ nanoparticles. *J. Superconduc. Novel Magnetism.* 32: 1791-1797.
17. Shalini C., Upadhyay M. K., (2012), Fruit-based synthesis of silver nanoparticles-an effect of temperature on the size of particles. *Recent Res. Sci. Technol.* 4: 41-44.
18. Sasikala C., Durairaj N., Baskaran I., Sathyaseelan B., Henini M., Manikandan E., (2017), Transition metal titanium (Ti) doped $LaFeO_3$ nanoparticles for enhanced optical structural and magnetic properties. *J. Alloys and Comp.* 712: 870-877.
19. Zhihong J., Wu S., (2004), Synthesis and characterization of monodisperse hematite nanoparticles modified by surfactants via hydrothermal approach. *Mater. Lett.* 58: 3637-3640.
20. Xu Y. Y., Zhao D., Zhang X. J., Jin W. T., Kashkarov P., Zhang H., (2009), Synthesis and characterization of single-crystalline α-Fe_2O_3 nano leaves. *Physica E: Low-dimens. Systems and Nanostruc.* 41: 806-811.
21. Abdelmajid L., Dkhil B., Gadri A., Ammar S., (2017), Control of the shape and size of iron oxide (α-Fe_2O_3) nanoparticles synthesized through the chemical precipitation method. *Results in Phys.* 7: 3007-3015.
22. Stjepko K., Ristić M., Petrović Z., Kratofil Krehula L., Mitar I., Musić S., (2019), Effects of Cu doping on the microstructural, thermal, optical, and photocatalytic properties of α-FeOOH and α-Fe_2O_3 1D nanoparticles. *J. Alloys and Comp.* 802: 290-300.
23. Killivalavan G., Prabakar A. C., Babu Naidu K. C., Sathyaseelan B., Rameshkumar G., Sivakumar D., Senthilnathan K., Baskaran I., Manikandan E., Ramakrishna Rao B., (2020), Synthesis and characterization of pure and Cu doped CeO_2

nanoparticles: photocatalytic and antibacterial activities evaluation. *Biointerf. Res. Appl. Chem.* 10: 5306–5311.
24. Lionel V., Beermann N., Lindquist S., Hagfeldt A., (2001), Controlled aqueous chemical growth of oriented three-dimensional crystalline nanorod arrays: Application to iron (III) oxides. *Chem. Mater.* 13: 233-235.
25. Jia D., Lu L., Yen W. M., (2002), Erbium energy levels relative to the band gap of gadolinium oxide. *Optics Communic.* 212: 97-100.
26. Biswajit C., Choudhury A., (2013), Room temperature ferromagnetism in defective TiO_2 nanoparticles: Role of surface and grain boundary oxygen vacancies. *J. Appl. Phys.* 114: 203906.
27. Guofeng W., Mu Q., Chen T., Wang Y., (2010), Synthesis, characterization, and photoluminescence of CeO_2 nanoparticles by a facile method at room temperature. *J. Alloys Comp.* 493: 202-207.
28. Abdelmajid L., Dkhil B., Gadri A., Ammar S., (2017), Control of the shape and size of iron oxide (α-Fe_2O_3) nanoparticles synthesized through the chemical precipitation method. *Res. Phys.* 7: 3007-3015.
29. Lian-Ying Z., Zhu J., (2003), Study on antimicrobial activity of chitosan with different molecular weights. *Carbohydrate Polym.* 54: 527-530.
30. Saptarshi C., Bandyopadhyay A., Sarkar K., (2011), Effect of iron oxide and gold nanoparticles on bacterial growth leading towards biological application. *J. Nanobiotechnol.* 9: 34-39.
31. Jennifer B., Baltrusaitis J., Chen H., Stebounova L., Wu C., Rubasinghege G., Imali A., (2014), Iron oxide nanoparticles induce pseudomonas aeruginosa growth, induce biofilm formation, and inhibit antimicrobial peptide function. *Environm. Sci.: Nano* 1: 123-132.
32. Gopinath K., Karthika V., Sundaravadivelan C., Gowri S., Arumugam A., (2015), Myogenesis of cerium oxide nanoparticles using Aspergillus niger culture filtrate and their applications for antibacterial and larvicidal activities. *J. Nanostruc. Chem.* 5: 295-303.
33. Jong-Whan R., Seok-In H., Hwan-Man P. P., (2006), Preparation and characterization of chitosan-based nanocomposite films with antimicrobial activity. *J. Agric. Food Chem.* 54: 5814-5822.
34. Parveen S., Wani A. H., Shah M. A., Devi H. S., Bhat M. Y., Koka J. A., (2018), Preparation, characterization and antifungal activity of iron oxide nanoparticles. *Microbial Pathog.* 115: 287-292.
35. Sudheer M., Sharma S. D., Katiyar S. K., (2006), Berberine, a natural product, induces G1-phase cell cycle arrest and caspase-3-dependent apoptosis in human prostate carcinoma cells. *Mol. Cancer Ther*. 5: 296-308.
36. Shouhu X., Wang F., Lai J. M., Sham K. W., Xiang Y. X., Siu-Fung Lee W., Jimmy C., Christopher C. H. K., Leung K., (2011), Synthesis of biocompatible, mesoporous Fe_3O_4 nano/microspheres with large surface area for magnetic resonance imaging and therapeutic applications. *ACS Appl. Mater. Interf.* 3: 237-244.
37. Esther A., Textor M., Reimhult E., (2011), Stabilization and functionalization of iron oxide nanoparticles for biomedical applications. *Nanoscale.* 3: 2819-2843.
38. Inbathamizh L., Mekalai Ponnu T., Jancy Mary E., (2013), In vitro evaluation of the antioxidant and anticancer potential of Morinda pubescens synthesized silver nanoparticles. *J. Pharm. Res.* 6: 32-38.
39. Krishnaraj C., Jagan E. G., Rajasekar S., Selvakumar P., Kalaichelvan P. T., Mohan N., (2010), Synthesis of silver nanoparticles using *Acalypha indica leaf* extracts and its antibacterial activity against water borne pathogens. *Colloids and Surf. B: Biointerf.* 76: 50-56.
40. Sathiya P., Ashok Kumar R., Geetha K., (2022), Synthesis and characterization of Gadolinium doped ZnS nanoparticles by chemical precipitation method and its antibacterial activity. *Int. J. Nano Dimens.* 13: 403-413.